Entry to the Stockholm Junior Water Prize 2025

Out of the Deep End:
Assessing the Impacts of Climate Change on Lake Winnipeg's Evaporation with Neural Networks

Aiyaan Mahir Faisal
Manitoba, Canada

2. Preliminary Matters

2a. Abstract

While evaporation currently accounts for approximately 15% of reservoir storage annually, climate change-induced temperature increases could exacerbate losses, a crucial consideration for hydropower generation, fisheries, irrigation, and lake ecosystems. This study assesses the impacts of climate change on evaporation over Lake Winnipeg, a vital lake for Manitoba, Canada, to inform future water resource management. However, inadequate weather data hinders the accurate evaporation estimation using current empirical equations, especially when analyzing the impacts of climate change based on limited climate model outputs. To address this gap, this study employs deep neural networks (DNNs), multilayer networks of artificial neurons capable of non-linear regression, as a solution to modelling evaporation with fewer variables while retaining sufficient accuracy. Using past climate data, six DNN models were trained on different input variables, with the most accurate model achieving an R^2 of 0.9970. Applying this model to simulated data from the CanLEADv1 climate ensemble dataset displayed that evaporation over Lake Winnipeg's southern basin would increase by roughly 30% by the end of the century, with significant increases noted during most months as soon as 2041-2060.

2b. Table of Contents

2c. Key Words

evaporation · deep neural networks · Penman evaporation equation · Lake Winnipeg · TensorFlow · global warming · global climate change · representative concentration pathway · hydroelectricity · hydroelectric generation potential · dam reservoirs · large open reservoirs · global warming · bias adjustment · Lower Nelson River Basin

2d. Abbreviations and Acronyms

DNN (Deep neural networks) · LNRB (Lower Nelson River Basin) · RCP (Representative concentration pathway) · R^2 (Coefficient of determination) · mm/d (Millimeters per day) · IPCC (International Panel on Climate Change) · T_{avg} (Average daily temperature) · T_{min} (Minimum daily temperature) · T_{max} · RH (Relative humidity) · u2 (2-meter windspeed) · R_a (Total incoming daily extraterrestrial radiation) · R_s (Measured net incoming shortwave/solar radiation)

2e. Acknowledgements

It is with the deepest appreciation that I give thanks to Mr. Michael Vieira, Dr. Faisal Islam, and Mr. Michael Kattenfeld for their help in completing this research. When I reached out to Mr. Vieira, the Climate and Meteorology Lead at Manitoba Hydro, for guidance on the existing knowledge gaps regarding the impacts of climate change on reservoir operations, he identified the climate change-induced evaporative loss as a primary gap and encouraged me to pursue this as a research topic. He also offered guidance on choosing appropriate climate scenarios and models and interpreting the simulated data from the selected climate model. Dr. Islam provided guidance on the machine learning and programming aspects of the project, helping me select appropriate analytical tools and programming libraries. Finally, I would like to thank Mr. Kattenfeld for his steadfast encouragement and support while preparing for the Canada Wide Science Fair, where the findings of this research was initially presented.

2f. Biography

Aiyaan Faisal is a grade eleven student at Grant Park High School in Winnipeg, Manitoba, Canada, who has varied interests in academic, community, and physical activities. He has been a regular participant in science fairs, including the Manitoba Schools Science Symposium and the national Canada Wide Science Fair, where he received multiple medals (gold, silver and bronze) along with special awards. In 2022, he received the Youth Can Innovate award, the only recipient of this award from Manitoba thus far. As for community service, Aiyaan has been a part of his school's student council for five years, serving as President during the 2023-2024 school year. Aiyaan is also a member of the Winnipeg chapter of E-Nable, a global non-profit dedicated to providing free 3D-printed prosthetics to those in need, aiding with virtual fitting and modelling of prosthetic hands. Aiyaan has been a dedicated member of his school's track and cross-country teams since the seventh grade and has run in provincial meets for 4x400m relay and 5km as well as a half marathon during Manitoba's first Truth and Reconciliation Run. Aiyaan was inspired to begin his research in 2024 around the topic of evaporation over Lake Winnipeg when he read about the overarching impacts of climate change on the hydropower generation potential in Manitoba, which resonated with him because of his interest in pursuing a career in renewable energy and electrical engineering in the future.

3. Introduction

Evaporation is a central component of water and energy exchange, driven by electromagnetic radiation, temperature gradient heat flows, and phase change heat flows [3]. Interactions between particles at the surface of a water body and the overlying dry air are influenced by these elements, which control the rate of evaporation [3]. Hydroelectric generation potential, the energy that can be generated in a dam's hydroelectric system, is dependent on the volume of water flow and the elevation change of water [3]. The greater the water flow and elevation change, the more electricity a hydropower plant can produce [5]. This means evaporation from open storage systems can diminish hydropower potential by restricting water volume and head difference [12]. While many studies have examined the impacts of changes in reservoir inflow brought on by climate change, few have examined the impacts brought about by climate change-induced evaporative fluxes [1]. From 1984 to 2016, temperatures in Canada have rapidly increased by 1.7 °C nationwide and 1.9 °C across the Prairies [2]. This is significant given the relationship between evaporation and temperature and the province of Manitoba's reliance on hydropower [5]. Under the high emission representative concentration pathway (RCP 8.5), from the IPCC's fifth climate report, the Canadian Prairies could experience an increase in annual mean temperature between 2.3 and 6.5 °C [2]. Further, strong scientific consensus suggests the warming rate in Canada is approximately twice the global mean [14]. A study examining climate change's impacts on water supply and hydropower generation indicated rising temperatures are expected to alter precipitation type and quantity, and affect its spatial and temporal distribution in future periods [5]. Given that evaporation and precipitation significantly affect reservoir levels, projected temperature rises must be carefully assessed in water-dependent regions [14]. Manitoba generates around 97% of its electricity via hydroelectric dams, and close to 70% of the province's hydropower generation capacity resides within the Lower Nelson River Basin (LNRB) [5]. Lake Winnipeg is one of the major lake water storage areas that impact LNRB operations, as the Nelson River starts off the lake [5]. Its release at the Jenpeg Station contributes roughly 67% of the annual flows for the cumulative Hudson Bay outlet [5]. Furthermore, increased evaporation rates could reduce available drinking water in communities that rely on surface water sources, diminishing freshwater supply for northern Canadian communities [9]. Environmental changes have altered the fragile thermodynamic relationships of northern ecosystems by shifting seasonal transitions, altering precipitation regimes, reducing snow and ice cover, and increasing exposure to solar radiation [9]. For these reasons, understanding the possible increases in evaporation brought on by temperature increases is a vital consideration for the management of Lake Winnipeg's water resources for the province of Manitoba.

Although an estimated 15% of the total water storage capacity is lost annually via evaporation, evaporation remains difficult to accurately quantify [4]. Several empirical methods for quantifying evaporation exist, relying on different theoretical foundations and input data, including mass balance, energy balance, and combined methods [3]. One study derived three simplified versions of the Penman evaporation equation, only requiring the use of routine weather data collected by most weather stations which all performed fairly well against the FAO CLIMWAT global climate dataset [14]. However, many climate models still do not output enough climate variables to use even these simplified methods for evaporation estimation. For this reason, this study turns to Deep Neural Networks (DNN), multilayer networks of artificial neurons, which are capable of modelling complex non-linear phenomena [6] as a possible solution to the issue of data availability. Because of the flexibility of DNN architecture, they have the ability to map complex processes to a high degree of accuracy, even when missing key variables [7]. DNNs learn by taking input variables, referred to as features, and passing them through layers of interconnected neurons [6]. Each neuron multiplies its inputs by assigned weights, sums the results, and passes the total through an activation function to produce its output. [6]. As the initial model weights are randomized, DNNs use a process called 'backpropagation' to readjust the weights across the gradient to minimize prediction error between its estimated and measured outputs (labels), using an evaluation metric such as mean-squared error [6]. Across many interactions of this process of predicting and adjusting the connection weights, referred to as epochs, a DNN can learn how to map complex non-linear processes [6].

4. Purpose

Given the established knowledge gap in understanding the extent of evaporation from large lakes [14], the potential effects of climate change in the Canadian Prairies [2], and Lake Winnipeg's importance to Manitoba's electricity production and economy [5], this study seeks to examine how climate change will impact Lake Winnipeg's evaporation. This was done by comparing evaporation over a historical period from 2010-2020 with evaporation from 2041-2100, split into three 20-year epochs to assess the extent of evaporation over time and determine when changes become significant. Comparisons were made on both a per-month and annual basis to better inform the planning of water resources. Moreover, given the additional limitations imposed by the lack of adequate weather data for modeling purposes, this study will be assessing the effectiveness of DNN-based models in evaporative loss prediction. This is done by training six DNN models on historical evaporation estimates using the Penman equation, selectively reducing input features and neurons to create models that omit certain inputs while retaining sufficient accuracy for planning needs.

5. Hypotheses

Mean monthly evaporation rates over Lake Winnipeg are expected to rise compared to historical averages, driven by global warming and the temperature-evaporation relationship, where higher temperatures intensify particle interactions and enhance evaporation. Due to their capacity to capture complex non-linear relationships, DNNs are well-suited for modeling evaporation and can yield results closely aligned with those produced by the Penman equation. Further, DNNs should be able to retain effectiveness even when fewer weather parameters are fed as input features, because of their flexible network structure and ability to effectively model complex phenomena even with limited inputs.

6. Materials and Methods

All data preparation, model training, and analysis were conducted on a Lenovo LOQ laptop. Past climatic data was taken from Visual Crossing, an online database of worldwide archived weather-station data. Specifically, for the southern basin of Lake Winnipeg, historic data for 2010-2020 was interpolated from nearby weather stations at the municipalities of Gimli and Victoria Beach for the point 50.75°N 96.75°W. Predicted weather data for 2041-2100 was taken from the CanLEADv1 Climate Ensemble, a grouping of several climate change scenarios under RCP 8.5, published by the Canadian Federal Government. The simulation used in this study was from the 'CanESM2_ALL-EWEMBI-MBCn/', specifically titled 'r1_rlilpl,' which accounted for all climate forcing, anthropogenic and natural, for North America from 1950-2100. This simulation used a single grid cell at 50.75°N, 96.75°W to compare evaporation estimates based on historical weather data with projections from DNN models for 2041-2100. The future period was divided into three 20-year intervals to track changes over time, using monthly mean evaporation rates (mm/d) as the primary metric.

Python codes were written to perform the calculation of evaporation via the Penman equation [5] for the historical period. Using this data and the TensorFlow 2.0 library, a Python script was written to generate the DNN models. The first model was trained on 7 input features, using the ReLU activation function and Adam optimizer in 500 epochs, running through 4018 daily records, and it had 2 hidden layers of neurons (14 x 7). Subsequent models featured fewer inputs and neurons, with the first hidden layer containing twice as many neurons as inputs, and the second hidden layer matching the number of input features.

6a. Historical Evaporation Period

Initially, historical climate measurements were taken directly from Visual Crossing, interpolated for the point 50.75°N 96.75°W based on weather stations at Gimli and Victoria Beach. These measurements included seven key climatic variables, relevant for the Penman equation: mean, minimum, and maximum temperatures (T, T_{min}, & T_{max}), relative humidity (RH), windspeed at a 2m height (u2), incoming extraterrestrial radiation (R_a), and measured net incoming solar radiation (R_s). A Python script was used to automate the process of reading measured weather data and applying it through the Penman equation (see Annex 1). Using daily records from 1 Jan. 2010 to 31 Dec. 2020, daily evaporation rates were estimated from 2010-2020 in terms of mm/day and summarized into monthly mean evaporation rates for this historical period. The mean annual evaporation was also estimated using the daily records for the entire period to serve as another metric for comparison.

The Penman equation required modifications since it was originally formulated for above-zero temperatures, to account for the sub-zero conditions typical of Manitoba's fall and winter months. Although reservoir losses due to sublimation are generally lower than those from evaporation, the prolonged sub-zero temperatures could make sublimation from the frozen lake surface more significant. To capture these effects, adjustments were made to the calculations for vapor pressure [8], the vapor pressure deficit [8], the slope of the saturation vapor pressure curve [10], and the latent heats of vaporization and sublimation [10].

6b. DNN Model Generation

The six DNN models used in this study were trained as follows. The data used for training the model came from the historical evaporation estimates generated with the Penman equation, with daily measured weather variables serving as input features and the estimated daily evaporation values acting as target or label data. Each of the models utilized 80% of the 4018 daily records for training, whereas the remaining 20% was used for model evaluation and testing. The activation function chosen was ReLU, or Rectified Linear Unit, for its simplicity and its ability to avoid vanishing gradients for model weights. Adam, or adaptive moment estimation, was chosen as the model optimizer for every model. A model optimizer is an algorithm that is used to adjust the weights and biases of the neural network to minimize the loss function, which in this project was Mean Squared Error (MSE). The initial learning rate, or the amount to which connection weights can be adjusted, was chosen to be 0.001 to avoid overfitting, Adam optimizer dynamically adjusts the learning rate to allow for faster and accurate learning. Each model was trained for 500 training cycles or epochs. R^2 was used to assess the models' predictive power at the end of training and during testing (significant deterioration of R^2 between training and testing would signal overfitting). While each model was trained in the same way, each had a different number of inputs and a different network structure. The first model trained, M0, had seven input variables, the same as the Penman method, and two hidden layers. The first layer contained 14 neurons – double the number of input variables, and the second layer had 7 neurons, matching the number of input variables. This convention is a widely used rule of thumb for DNNs, the same convention was used for all other models as it helped to diminish the risk of overfitting while maintaining strong predictive power.

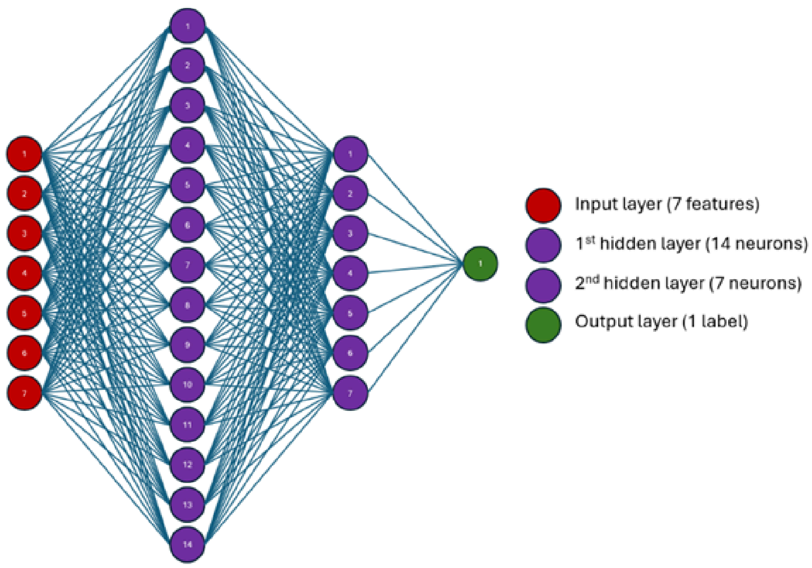

Fig 1 displays the DNN model structure for M0 with 7 features (input nodes).

6c. Future Evaporation

While future climate data was initially taken directly from the CanLEADv1 Climate Ensemble dataset, further augmentation and bias correction were required before it was used as input for the trained DNN models. Raw data was available in netCDF file format and Python script was written to automate the extraction and conversion of data from netCDF to CSV format. Further, the CanLEADv1 generated wind speed data exhibited a clear bias, significantly underestimating 'u2' (wind speed at 2m) and lowering its variance, apparent when compared with measured wind speed data. For this reason, bias adjustment was done by shifting the mean of the windspeed data toward the historical average, while also correcting for the variance. (No corrections were required for temperature, relative humidity, and radiation data from CanLEADv1).

The first DNN model, M0, was fed all seven input variables on a daily basis from 2041-2100 to generate model-predicted daily evaporation data. As was done with historic evaporation estimates, these daily model-predicted values were summarized into monthly mean evaporation rates and mean annual evaporations. As mentioned earlier, the future period was broken down into three smaller segments (2041-2060, 2061-2080, and 2081-2100) to allow for the successive charting of changes in evaporation over time.

7. Results and Observations

7a. Past Evaporation

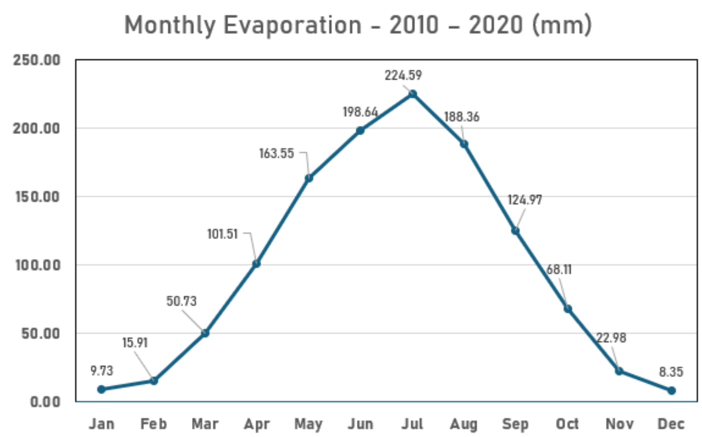

Fig 2 displays the average evaporation that occurs during each month of the year in mm over the surface of the lake for the historical baseline period (2010-2020).

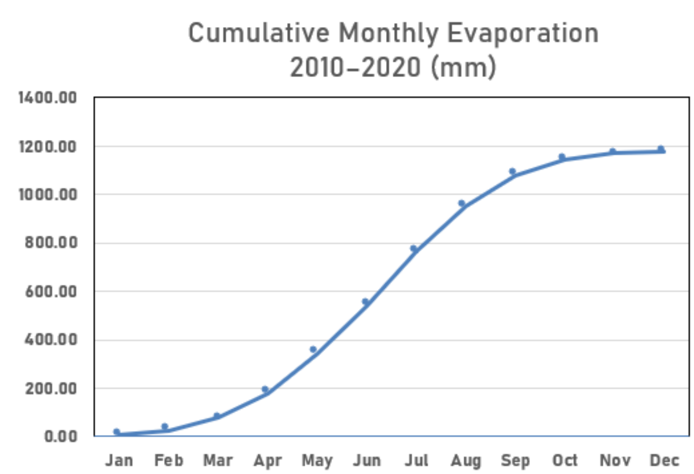

Fig 3 displays the average cumulative annual evaporation in the historical period, totalling 1187.3 mm over the southern basin of Lake Winnipeg.

These baseline results show that monthly evaporative losses range between 8-225 mm in a given month, with a maximum occurring in July. In addition, the cumulative losses come up to 1187.3 mm on an annual basis. With the corrections made for sub-zero conditions and sublimation, we can see that winter months do contribute some amount to the annual losses, with around 54mm of the surface being lost from November to January.

7b. Model Performance Summary

Model stage	Hidden layer	R^2	MSE
M0 (T_{max} , T_{min}, T_{avg}, RH, R_a, R_s, u2)	14 x 7	0.9970	0.0231
M1 (T_{max} , T_{min}, RH, R_a, R_s, u2)	12 x 6	0.9963	0.0297
M2 (T_{max} , T_{min}, RH, R_a, R_s)	10 x 5	0.9647	0.2812
M3 (T_{max} , T_{min}, RH, R_a, R_{S_HS})	10 x 5	0.9449	0.4130
M4 (T_{max} , T_{min}, RH)	6 x 3	0.8934	0.7600
M5 (T_{max} , T_{min})	4 x 2	0.7949	1.2886

Fig 4 summarizes the performance of the DNN models generated with different numbers of input variables. The only exception to the trend of removing variables is M3, where R_s was replaced with R_{S_HS}, an estimate using the Hargreaves-Samani Equation [11]. Note that R_a was always calculated directly based on the day of the year (Julian day).

The most accurate models were, as expected, M0 and M1, which were fed all the same measured variables that the Penman method required, but did not require the various calibrated coefficients described in Annex 1. For M0, an R^2 of 0.9970 means the model was capable of explaining 99.70% of the total variance of Penman evaporation estimation, essentially indistinguishable from the empirical methods' accuracy. It appears that T_{avg} has very little predictive power, due to the negligible decrease of R^2 between M0 and M1 (0.9970 vs 0.9963). M3 strikes the best balance between accuracy and data requirements. Two of the input variables contained in M3 are estimated (R_a and R_{S_HS}), which means that with just three input variables, an R^2 of 0.9449 was achieved via a DNN.

7c. Future Evaporation

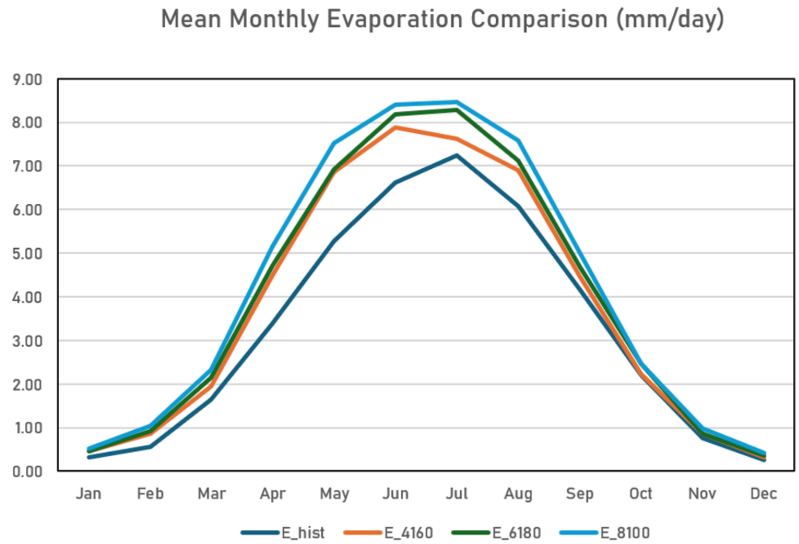

Fig 5 shows a direct comparison of the mean monthly evaporation rate (in mm/day) between historical evaporation ‘E_hist’ and each segment of the 2041-2100 future period. ‘E_4160’ encodes evaporation from 2041-2060, and subsequent periods are described in the same format. For each subsequent period, it is evident that the monthly means are gradually increasing and the trend is clearly noticeable for the months of March to September.

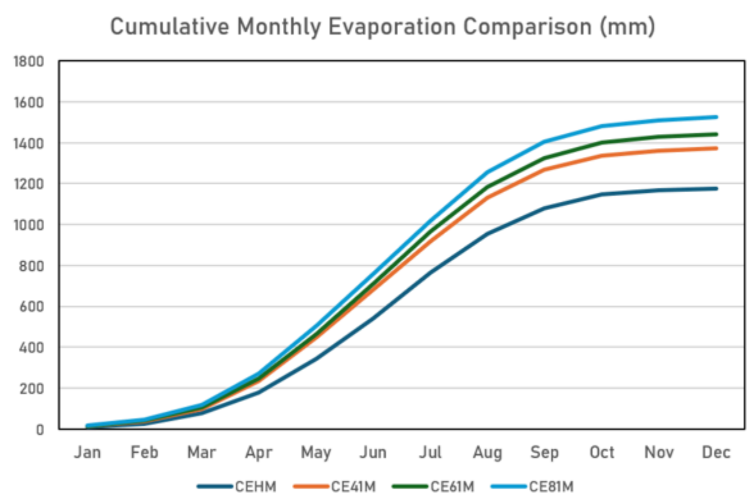

Fig 6 shows a direct comparison of the cumulative annual average evaporation in different periods. The cumulative values illustrate the projected rise in mean annual evaporation (mm) across various time periods.

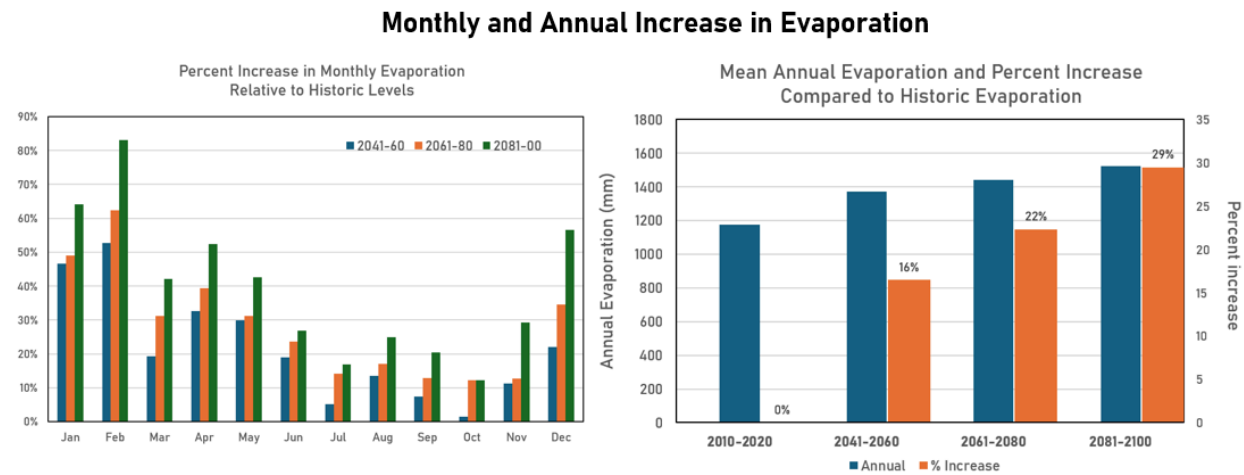

Fig 7 shows the percent increase in both monthly evaporation rate and cumulative annual evaporation.

As shown in Figs. 4 and 5, evaporation over the surface of the southern basin of Lake Winnipeg will increase in the future, driven by the temperature increase brought on by climate change. The greatest increases in evaporative loss occur in spring and summer months, from April to July, with monthly mean evaporation rate increases ranging between 12% and 82% by the end of the century. Winter months experienced a high percentage increase due to negligible historical evaporation compared to minor future evaporation. (0.5mm vs 1.3mm). Comparing the cumulative annual evaporative loss, an increase of 29% was found when comparing 2081-2100 against 2010-2020.

7d. Statistical Analysis

Given the increases in monthly evaporation rates in all months under the predicted changes in climate variables, verification of the statistical significance of these changes was required to draw conclusions. A t-test for comparing means was desired, but since the sample sizes were small, with 11 different monthly mean evaporation rates for 2010-2020 and 20 for each of the future periods, normality tests were conducted before choosing a method for assessing statistical significance.

	2041-2060		2061-2080		2081-2100	
Month	Shapiro-Wilk p-value	Normality Assumption	Shapiro-Wilk p-value	Normality Assumption	Shapiro-Wilk p-value	Normality Assumption
jan	0.67134	Accepted	0.014064984	Rejected	0.185708433	Accepted
feb	0.83504	Accepted	0.175549562	Accepted	0.650423098	Accepted
mar	0.04330	Rejected	0.095863234	Accepted	0.909865703	Accepted
apr	0.55948	Accepted	0.779870432	Accepted	0.021794102	Rejected
may	0.88100	Accepted	0.57275287	Accepted	0.988949117	Accepted
jun	0.67109	Accepted	0.397919158	Accepted	0.761288482	Accepted
jul	0.81067	Accepted	0.123691121	Accepted	0.904072582	Accepted
aug	0.88962	Accepted	0.152388986	Accepted	0.188377924	Accepted
sep	0.09871	Accepted	0.525983362	Accepted	0.739417017	Accepted
oct	0.96809	Accepted	0.12104981	Accepted	0.152718971	Accepted
nov	0.61826	Accepted	0.416476956	Accepted	0.208254498	Accepted
dec	0.01677	Rejected	0.291319395	Accepted	0.562193518	Accepted

Fig 8 displays the Shapiro-Wilk Normality Test results for monthly mean distributions from 2041-2060, 2061-2080, and 2081-2100. The 'Shapiro-Wilk p-value' column indicates whether the data deviates from a normal distribution; p-values below 0.05 suggest rejecting the null hypothesis of normality. Any rejected distributions are marked with red text under the 'Normality Assumption' column.

Because of the non-normality of several monthly mean distributions, the Mann-Whitney U test was employed for assessing statistical significance. The Mann-Whitney U test is a non-parametric statistical test, meaning it only requires that the samples are independent and that the data points are either ordinal or continuous. Figure 9 shows the results from the Mann-Whitney tests.

Month	MH_4160_U	MH_4160_P	MH_6180_U	MH_6180_P	MH_8100_U	MH_8100_P
jan	11	4.76867E-05	6	1.9276E-05	4	1.3265E-05
feb	7	2.31798E-05	0	6.15969E-06	0	6.15969E-06
mar	41	0.004682508	19	0.000186677	12	5.68788E-05
apr	12	5.68788E-05	3	1.0977E-05	1	7.48019E-06
may	5	1.60036E-05	14	8.05269E-05	1	7.48019E-06
jun	15	9.55825E-05	15	9.55825E-05	12	5.68788E-05
jul	75	0.154338852	18	0.000158295	12	5.68788E-05
aug	29	0.000888845	25	0.000485414	10	3.9915E-05
sep	73	0.131824973	43	0.006041354	41	0.004682508
oct	93	0.495731454	49	0.012496261	66	0.072502924
nov	61	0.045244109	46	0.008750012	30	0.001029829
dec	29	0.000888845	19	0.000186677	9	3.33556E-05

Fig 9 shows the results of applying the Mann-Whitney U-tests. Any values below the chosen power (0.05) are considered significant. Each column is coded as 'MH' (monthly historical) followed by the future period being compared, and then either 'U' or 'P' depending on which statistic is in the column.

Using the Mann-Whitney U test, it was found that even in the closest future period, nine of the 12 months experienced significant increases. As temperatures rise into the future, all months of the year experience significant increases in 2061-2080, and in 2081-2100, 11 out of the 12 months experience significant increases.

7e. Scope of Study

The findings of this study were based on the results or outputs from one specific grid cell of the CanLEADv1 climate model representing an extreme version of climate change. Further, this study considered only one point, the midpoint of the southern Lake Winnipeg basin for estimating past evaporation. Given Lake Winnipeg's estimated surface area of 24 514 km^2, climate impacts will differ between northern and southern basins. Since the resolution of CanLEADv1's grid is around 0.5 degrees in both longitude and latitude, this translates to roughly 1800 km^2 at a latitude of 50.75°N. Therefore, examining a single cell represents a fraction of the lake surface. For this reason, this study's findings do not accurately represent the impact of climate change across the entire lake. While analyzing all cells on the lake surface could resolve this issue, it would require establishing some formula for partial-cell evaporation and accessing future and historical data for multiple cells. Additionally, wind speed bias in CanLEADv1 limits its direct use because the results are tied to the method chosen for bias adjustment, which may vary with alternate approaches. Furthermore, it is important to recognize that forecast accuracy generally decreases the farther it extends into the future. This is especially relevant when interpreting projections for 2081–2100, which are likely to deviate more from actual future conditions compared to those for 2041–2060. Finally, although the structure of DNN models was adjusted appropriately for the number of features, the study could have explored other network configurations (different numbers of layers and nodes) along with more formal methods for hyperparameter tuning.

8. Conclusions

Using M0 on future climatic data from CanLEADv1, mean monthly evaporation was found to increase in the future when compared against historical averages. Monthly mean evaporation rates increased between 12% and 82% by the end of the century, and annual cumulative evaporative loss increased by 29% by the end of the century. The non-parametric

Mann-Whitney test confirmed the significance of these increases in 9 out of 12 months for 2041-2060, and in all months for 2061-2080. Significant increases were also noted in 11 out of 12 months in 2081-2100. DNN-based evaporation prediction models were found to be as accurate as the Penman equation, during model training and testing, with the full 7-variable model achieving an R^2 of 0.9970. Reduced DNN models, with fewer input variables (features), remained effective in predicting evaporation, with the R^2 degrading from 0.9963 with six variables to 0.7949 with just two variables (T_{max} & T_{min}). This means that a reduced model with just two inputs could still explain nearly 80% of the total variance in the dependent variable, evaporation. Furthermore, M3 was found to be very economical, requiring only three input variables (the other two input variables are estimated from these three and empirical equations) and it produced an impressive R^2 of 0.9449.

9. Discussion

The findings of this study, though specific to the grid resolution and simulation scenario within CanLEADv1's outputs, underscore the potential for drastic increases in evaporation from Lake Winnipeg due to climate change. A projected 30% rise in annual evaporative loss requires careful consideration in hydropower dam operations, as it could impact water availability and energy production. Complementary research on the Lower Nelson River System, using a different methodology, revealed that evaporative loss would intensify during drier months, while wetter months could see increased precipitation [5]. This interplay between evaporation and precipitation is crucial as higher precipitation could mitigate some of the evaporative losses, making a balanced assessment necessary to determine the net climate change impact. Beyond hydropower, Lake Winnipeg supports fisheries, recreation, and ecosystems, making its vulnerability to climate change an issue that extends across multiple economic and environmental sectors. Understanding the broader consequences of these changes opens the door for more advanced studies in the future that could refine predictions and guide long-term adaptation strategies.

10. References

[1] Adeloye, A. J., Nawaz, N. R., & Montaseri, M. (1999). Climate change water resources planning impacts incorporating reservoir surface net evaporation fluxes: A case study.

International Journal of Water Resources Development, *15*(4), 561–581. https://doi.org/10.1080/07900629948763

[2] Bush, E., & Lemmen, D.S. (Eds.). (2019) *Canada's changing climate report*. Government of Canada.

[3] Dingman, L. (2008). *Physical Hydrology, 3rd Edition*. Waveland Press, Inc.

[4] Helfer, F., Lemckert, C., & Zhang, H. (2012). Impacts of climate change on temperature and evaporation from a large reservoir in Australia. *Journal of hydrology*, *475*, 365-378.

[5] Kim, S. J., Asadzadeh, M., Stadnyk, T. A. (2022). Climate change impact on water supply and hydropower generation potential in northern Manitoba. *Journal of Hydrology: Regional Studies, 41*(101077). https://doi.org/10.1016/j.ejrh.2022.101077

[6] Krohn, J., Beyleveld, G., Bassens, A. (2020). Deep Learning Illustrated. Pearson Education, Inc.

[7] Lee, W. M. (2019). Python Machine Learning. Wiley.

[8] Murray, F. W. (1967). On the computation of saturation vapour pressure. *Journal of Applied Meteorology, 6*, 203–204.

[9] Medeiros, A. S. (2017). Water security for northern peoples: Review of threats to Arctic freshwater systems in Nunavut, Canada. *Regional Environmental Change*, *17*, 635-647. https://doi.org/10.1007/s10113-016-1084-2

[10] Rogers, R. R., & Yau, M. K. (1989). *A short course in cloud physics* (3rd ed.). Pergamon Press.

[11] Shahidian, S., Serralheiro, R. P., Serrano, J., & Teixeira, J. L. (2013). Parametric calibration of the Hargreaves–Samani equation for use at new locations. Hydrological Processes, 27(4), 605-616.

[12] Stadnyk, T. A., & Déry, S. J. (2021). Canadian continental-scale hydrology under a changing climate: A review. *Water*, *13*(7), 906. https://doi.org/10.3390/w13070906

[13] U.S. Energy Information Administration. (n.d.). *Hydropower explained.* https://www.eia.gov/energyexplained/hydropower/#:~:text=The%20volume%20of%20the%20water,a%20hydropower%20plant%20can%20produce

[14] Valiantzas, J. D. (2006). Simplified versions for the Penman evaporation equation using routine weather data. *Journal of Hydrology, 331*(3-4), 690-702. https://doi.org/10.1016/j.jhydrol.2006.06.012

11. Bibliography

Aminzadeh, M., Friedrich, N., Narayanaswamy, S., Madani, K., & Shokri, N. (2024). Evaporation loss from small agricultural reservoirs in a warming climate: An overlooked component of water accounting. *Earth's Future*, *12*(1). https://doi.org/10.1029/2023EF004050

Ghasemi, A., & Zahediasl, S. (2012). Normality tests for statistical analysis: a guide for non-statisticians. *International journal of endocrinology and metabolism*, *10*(2), 486–489. https://doi.org/10.5812/ijem.3505

Manitoba Hydro. (2020). *Manitoba Hydro's climate change report.* https://www.hydro.mb.ca/docs/corporate/climate_change_report_2020.pdf

Nevermann, H., Aminzadeh, M., Madani, K., Shokri, N. (2024). Quantifying water evaporation from large reservoirs: Implications for water management in water-stressed regions. *Environmental Research, 262*(1). https://doi.org/10.1016/j.envres.2024.119860

Penman, H. L. (1948). Natural evaporation from open water, bare soil and grass. *Proceedings of the Royal Society of London. Series A. Mathematical and Physical Sciences*, *193*(1032), 120-145.

Raty, O., Raisanen, J., & Ylhaisi, J. S. (2014). Evaluation of delta change and bias correction methods for future daily precipitation: intermodel cross-validation using ENSEMBLES simulations. *Climate Dynamics, 42*, 2287-2303. https://doi.org/10.1007/s00382-014-2130-8

Rosenberry, D. O., Winter, T. C., Buso, D. C., Likens, G. E. (2007). Comparison of 15 evaporation methods applied to a small mountain lake in northeastern USA. *Journal of Hydrology, 340*, 149-166. https://doi.org/10.1016/j.jhydrol.2007.03.018

12. Annex I. Penman Calculations + Modifications for Subzero Temperatures

The following contains all the steps required in the simplified Penman method for calculating daily evaporation over an open-water surface using weather station data [14]. Corrections for subzero temperatures allowed for sublimation to be accounted for as well. These corrections were made for the calculation of mean saturation vapour pressure (E_s), vapour pressure deficit of average daily temperature (D), latent heat of vaporization (λ), and the slope of the vapour pressure curve (Δ). The correction for E_s is an adjusted form of Tenten's equation for saturation vapour pressures below 0 °C [8]. This correction is present in both the calculation of average E_s and for D, which is calculated using E_s. λ for water is greater at subzero temperatures than above zero temperatures, because it is the sum of the latent heat of fusion and the latent heat of vaporization to account for sublimation [10]. The exact value was derived in part using *A Short Course in Cloud Physics* [10], and further recommendations in *Physical Hydrology* [3]. Δ is derived from the Clausius-Clapeyron equation but altered and approximated for subzero temperatures as discussed in *A Short Course in Cloud Physics* [10]. These approximations allowed for the calculation of total reservoir loss due to evaporation even at below-zero temperatures.

Step & Variable	**Equation for Above Zero Temperatures**	**Alternate Equation for Subzero Temperature**
1) R_{ns}, net incoming short wave radiation	$(1 - \alpha) \cdot R_s$, where α is the reflection coefficient/albedo (0.08 for open water) & R_s is measured or estimated incoming solar radiation in $MJ/m^2/d$	**N/A**
2) E_s average, mean saturation vapor pressure in mmHg	$E_{s\,MAX} = 0.611 \cdot \exp((17.27 \cdot T_{max})/(T_{max} + 273.3)$ $E_{s\,min} = 0.611 \cdot \exp((17.27 \cdot T_{min})/(T_{min} + 273.3)$ $E_{s\,avg} = (E_{s\,min} + E_{s\,max}) / 2$	$E_{s\,MAX} = 0.611 \cdot \exp((21.87 \cdot T_{max})/(T_{max} + 265.5)$ $E_{s\,min} = 0.611 \cdot \exp((21.87 \cdot T_{min})/(T_{min} + 265.5)$ $E_{s\,avg} = (E_{s\,min} + E_{s\,max}) / 2$
3) E_a average, effective vapour pressure	$E_{s\,avg} \cdot RH / 100$	**N/A**
4) D_{avg}, mean vapor pressure deficit	$D_{s\,avg} = E_{s\,avg} - E_{a\,avg}$	**N/A**
5) D, mean vapor pressure deficit of average temperature (T) (not to be confused with step 5)	a) $E_s = 0.611 \cdot \exp((17.27 \cdot T)/(T + 273.3)$ b) $E_s \cdot RH / 100$ c) $D_{s\,avg} = E_{s\,avg} - E_{a\,avg}$	a) $E_s = 0.611 \cdot \exp((21.87 \cdot T) / (T + 265.5)$ b) Same c) Same

6) λ**,** latent heat of vaporization	$\lambda = 2.501 - (2.361 \times 10^{3}) \cdot T$	$\lambda = 2.8351$
7) P, pressure in kPa	$P = 101.3 \cdot (1 - 0.0065 \cdot Z / 293)^{5.26}$, where Z is altitude from sea level, 222 for this calculation	**N/A**
8) γ**,** psychometric constant	$\gamma = 0.0016286 \cdot P / \lambda$	**N/A**
9) $\mathbf{R_{SO}}$, clear sky radiation	$R_{SO} = (0.75 + 2 \times 10^{-5} \cdot Z) \cdot R_A$, where R_A is extraterrestrial radiation (MJ/m^2/d)	**N/A**
10) $\dot{\varepsilon}$**,** net emissivity between the atmosphere and the ground	$\dot{\varepsilon} = (0.34 - 0.14\sqrt{E_a}$	**N/A**
11) f, adjustment factor for cloud cover	$f = (1.35 \times R_s / R_{SO} - 0.35)$, where R_S is measured solar radiation in (MJ/m^2/d)	**N/A**
12) $\mathbf{R_{nL}}$**,** net outgoing long wave radiation	$R_{nL} = f \cdot \dot{\varepsilon} \cdot \sigma\, (T + 273.2)^4$, where T is conventionally calculated as the average of T_{max} and T_{min} (not the same thing as just T from before)	**N/A**
13) Δ**,** slope of saturation vapor pressure curve	$\Delta = 4908 \cdot E_s / (T + 237.3)^2$	$\Delta = 4908 \cdot E_s / (T + 265.5)^2$
14) $\mathbf{R_n}$**,** net radiation at surface (MJ/m^2/d)	$R_n = R_{ns} - R_{nL}$	**N/A**
15) f_u**,** wind function	$f_u = a_U + b_U \cdot u$, where a_U is 0 for the Linacre Wind Function [14], b_U = 0.536, and u is wind speed measured over a 2m height	**N/A**
16) E_PEN, potential evaporation calculated using the 1948 Penman equation (mm/d) [5]	$E_{PEN} = \frac{\Delta}{\Delta + \gamma} \cdot \frac{(R_n)}{\lambda} + \frac{\gamma}{\Delta + \gamma} \cdot \frac{6.43(f_U)D}{\lambda}$ All variables have been calculated in previous steps	**N/A**

Fig 10 lays out the steps required for Valiantazas's method of approximating the Penman Equation [14], with added accommodations for subzero temperatures taken from *Physical Hydrology* [3] and *A Short Course in Cloud Physics* [10], laid out sequentially.